To the Graduate Council:

I am submitting herewith a thesis written by Jawaharlal Prasad entitled "Mechanisms of Agglomeration of Fine Particles in a Magneto-hydrodynamic System." I recommend that it be accepted in partial fulfillment of the requirements for the degree of Master of Science, with a major in Chemical Engineering.

Lloyd W. Crawford, Major Professor

We have read this thesis
and recommend its acceptance:

Accepted for the Council:

Vice Chancellor
Graduate Studies and Research

MECHANISMS OF AGGLOMERATION OF FINE PARTICLES IN A MAGNETOHYDRODYNAMIC SYSTEM

A Thesis

Presented for the

Master of Science

Degree

The University of Tennessee, Knoxville

Jawaharlal Prasad

August 1981

To my grandfather,

Shri Hiralal Sah

ACKNOWLEDGMENTS

The author acknowledges with deep gratitude the valuable suggestions, guidance and encouragement given by his Major Professor, Dr. Lloyd W. Crawford, during the one year of graduate work. Dr. Crawford's infinite patience throughout the study is greatly appreciated. The author is also very grateful to Mr. S. S. Strom, Dr. J. J. Perona, and Mr. T. E. Dowdy for their valuable comments and guidance.

Sincere thanks are extended to Mr. N. S. Vidyasagaran, Ms. Margaret Wilson and Mr. Guy Materi and his wife, Cathy, for their words of encouragement during the time of this graduate work.

Thanks are also due to Mrs. Jeannie Harper for having typed the thesis so carefully.

The work reported herein was supported by the United States Department of Energy, Contract No. DE-AC01-79ET10815.

ABSTRACT

A model has been developed in order to explain the discrepancy between Im's theoretical prediction of particle size distribution and that obtained experimentally at The University of Tennessee Space Institute (UTSI), Tullahoma, Tennessee, for particulate emissions from a magnetohydrodynamic (MHD) system.

Agglomeration by thermophoresis acting between different sized particles has been employed to explain this discrepancy. The model explains successfully a significant portion of this discrepancy in terms of lower mass fraction of fine particles present in the measured particle size distribution as postulated.

TABLE OF CONTENTS

LIST OF TABLES

LIST OF FIGURES

NOMENCLATURE

A	Cross-sectional area
A'	Constant, 1.2
A, A_R	Reciprocal relaxation time
b	Buffer layer thickness
B, B_R	Mobility
B'	Constant, 0.41
C'	Constant, 0.88
C_A	Concentration of particles
C_{A_0}	Initial concentration of particles
C_{AIN}	Inlet concentration of particles
C_{AOUT}	Outlet concentration of particles
C_m	Momentum exchange coefficient
C_p	Specific heat of gas at constant pressure
C_s	Thermal slip coefficient
C_t	Temperature jump coefficient
Cu	Cunningham factor
ds	Elemental surface area
D	Tube diameter
D_{BP}	Diameter of large particle
$\hat{D}(b)$	Effective turbulent diffusion velocity
$\mathcal{D}$	Diffusion coefficient
$\mathcal{D}_e$	Particulate eddy diffusivity
f	Friction coefficient factor
f'	Frequency of oscillation

F_t	Thermophoretic force
F_v	Millikan drag force
g	Acceleration due to gravity
G	Mass flux
h	Heat transfer coefficient
J	Particle flux toward the surface
k	Boltzmann constant
k_g	Thermal conductivity of gas
k_m	Thermal conductivity of metal
k_p	Thermal conductivity of particle
k_s	Surface roughness
K_1	Wave number
Kn	Knudsen number, ratio of gas mean free path and particle radius
ℓ	Distance between two large particles
ℓ'	Laminar sublayer thickness
ℓ_w	Wall thickness
L	Length of component
$L_{ij}^{(T)}$	Collision rate density
$\dot{m}$	Total mass flow rate
$\dot{m}_{AR}$	Mass flow rate
$\dot{m}_{coal}$	Coal flow rate
m_g	Mass of gas
m_p, m_k	Mass of particle
$\dot{m}_{O_2}$	Oxygen flow rate
$\dot{m}_{N_2}$	Nitrogen flow rate

M_g	Molecular weight
$\vec{n}_A, n_{AR}$	Mass flux
n_i, n_j	Number density of species i,j
n_{io}	Initial number density of species i
N_A	Number of particles per unit mass
Nu	Nusselt number
p	Pressure
P'	Perimeter
Pr	Prandtl number
q	Mass average gas velocity based on center of mass of the gas, relative to fixed coordinate system
$\dot{q}$	Heat flow
$\dot{q}''$	Heat flux
r, r_i, r_j	Radius of particle
r_{ij}	$r_i + r_j$
r_{bp}	Radius of large particle
r_{sp}	Radius of fine particle
r_t	Radius in the tube
R	Coordinate specifying distance from center of a collecting particle
R'	Universal gas constant
Re	Reynolds number based on steady-state velocity
Re_v	Reynolds number based on velocity difference between gas and particle
R_t	Radius of a tube
S	Stopping distance

Sc	Particulate Schmidt number
St	Stanton number
t	Flow time
T	Temperature
T_g	Average gas temperature
T_{g1}, T_1	Inlet gas temperature
T_{g2}, T_2	Outlet gas temperature
T_o	Mean temperature in the vicinity of particle
T_p	Particle temperature
T_w	Wall temperature
T_{water}	Water temperature
u	Velocity
$\overline{u}_g$	Mean molecular velocity
u_g	Fluctuating gas velocity
u_o	Maximum gas velocity
u_p	Particle velocity
U_T	Thermophoretic velocity
V	Particle diffusion velocity
$\overline{V}$	Steady-state velocity
V^*	Friction velocity
x,y	Space coordinate

Greek Letters

α	Thermal diffusivity
μ_g	Dynamic viscosity of gas
ρ_g	Density of gas

ρ_i, ρ_p	Density of particle
ν	Kinematic viscosity of gas
λ	Mean free path
ω	Angular frequency
ω_A, ω_A'	Mass fraction
η, ψ, ψ_{TOT}	Collection efficiency
τ	Constant, 0.42
σ	Stefan-Boltzmann constant
ε	Emissivity
ε_t	Energy dissipated per unit mass
ε'	Eddy diffusivity of gas
ϕ	Lag
∇	Gradient
Δ, δ	Increment
$\sum$	Summation

CHAPTER I

INTRODUCTION

Purpose of the Study

Kwan H. Im and Paul M. Chung [1][1] have carried out calculations to predict the particle size distribution in the different components of a magnetohydrodynamics (MHD) plant. Im and Chung [1] have discussed the formation of slag droplets from vapor and the evolution of the droplet sizes in the different components of an MHD plant. Figure 1 shows a slag particle size spectrum as calculated by Im et al. [2]. This plot of particle number density versus particle radius is converted into a plot of mass fraction versus logarithm of radius. Im's model is shown in Figure 2 and described in Appendix A.

However, the theoretical predictions of the particle size are not in good agreement with the particle size measured experimentally (Figure 2) at The University of Tennessee Space Institute (UTSI), Tullahoma, Tennessee [3].

The test runs are referred to as TP37-08, TP37-09, TP37-11, and TP37-12 (Figure 2). The main variation in the series of runs TP37-08 to TP37-12 is in the coal-potassium carbonate ratio in the coal mixture, being higher for test TP37-08 and lower at the higher test numbers. There was also some variation in coal-oxygen ratio, but not regularly. There is no reason apparent for the size variation

---

[1]Numbers in brackets refer to similarly numbered references in the Bibliography.

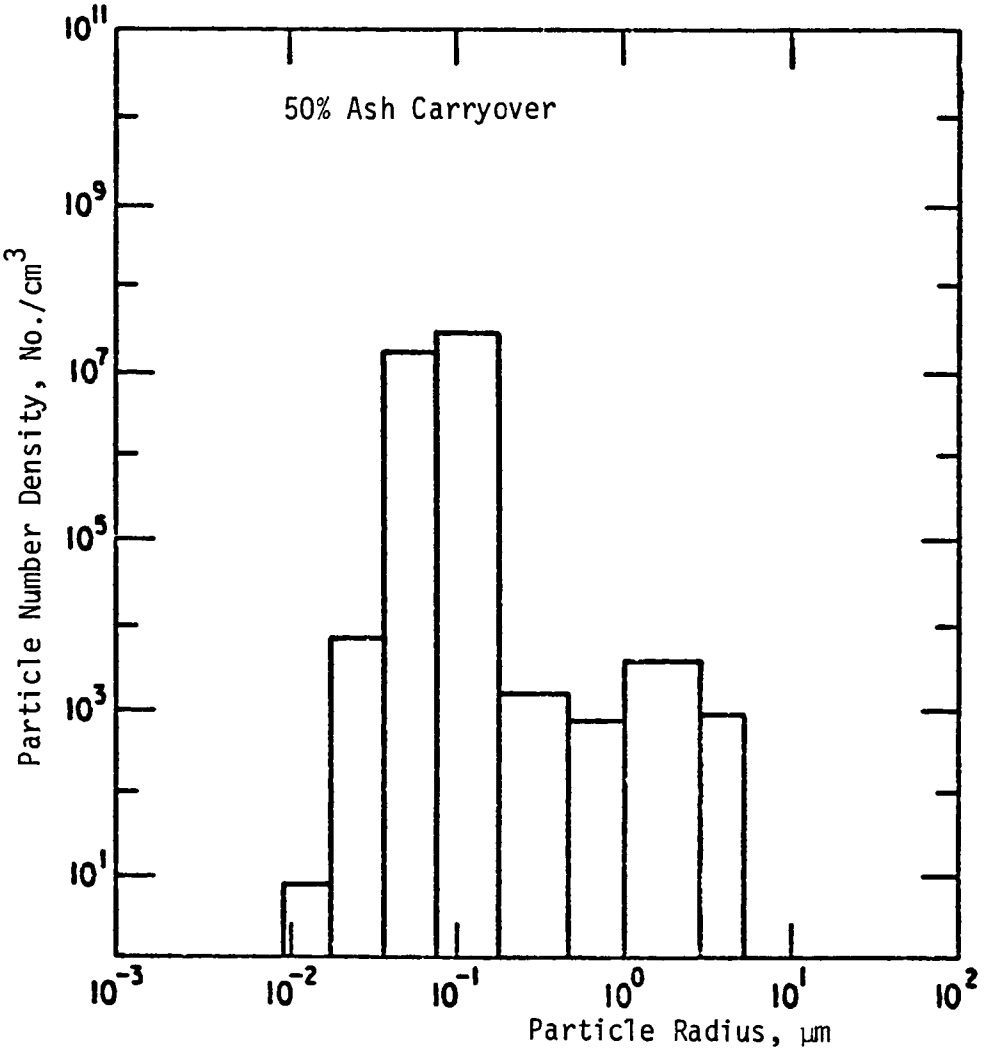

Figure 1. Slag particle size spectrum.

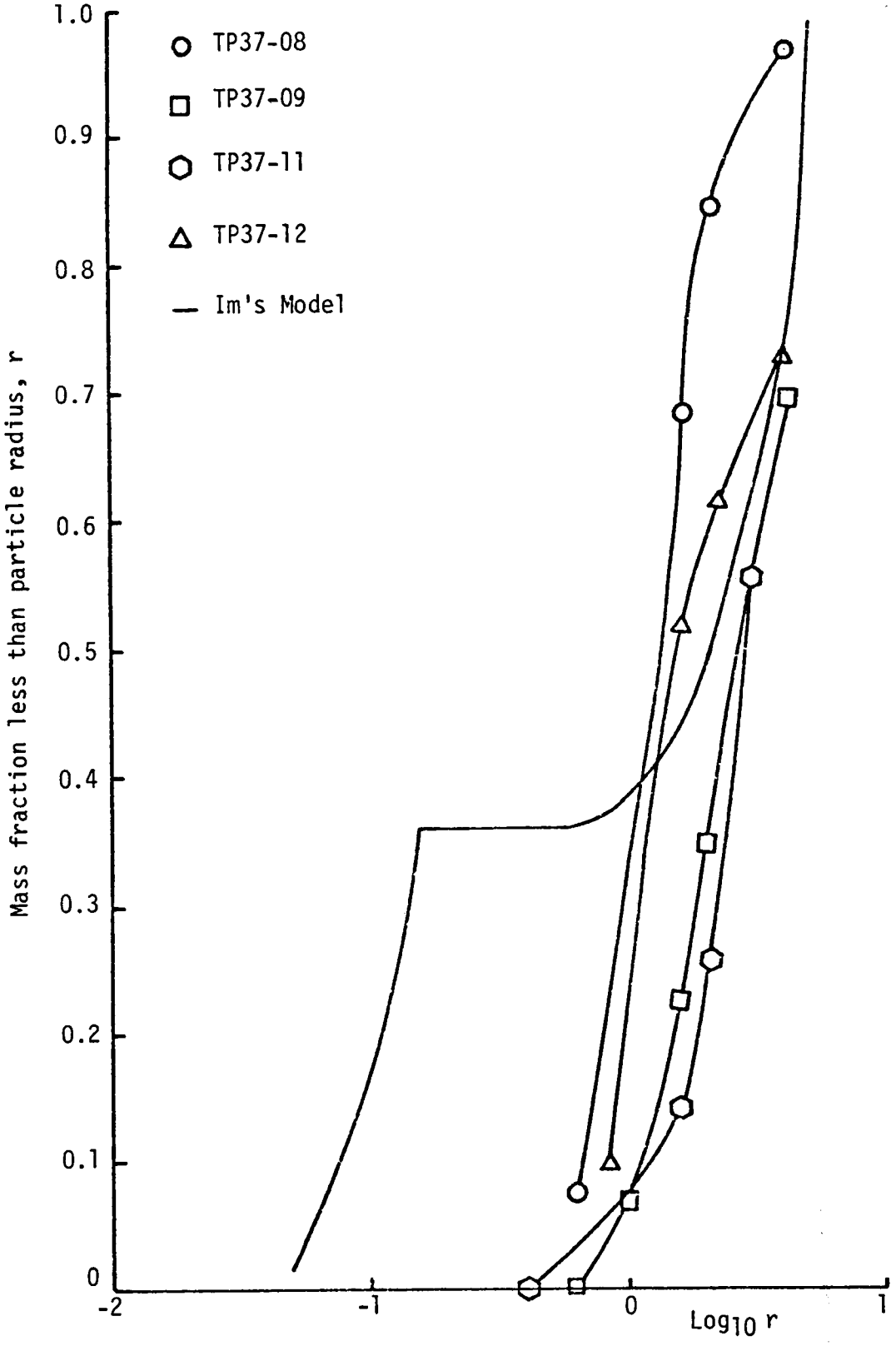

Figure 2. Particle size distribution of Im's model and those obtained experimentally at UTSI.

among the runs. The exact values are given in Appendix A. It is clear, however, that in no case was an appreciable fraction less than 0.5 μm in radius.

The difference between the theoretical distribution and measured distribution lies in the much lower fraction of submicron particles in the measured distribution. It is intended in this work to attempt to explain the discrepancy that exists between the observed particle size distribution and the theoretically predicted size distribution. For this reason, mechanisms which might lead to agglomeration of very fine particles are to be studied.

Need for the Study

In the open cycle coal-fired MHD plant, coal is burned to provide the high temperature required to effect dissociation of the seeding agent and subsequent formation of the plasma. Although coal serves a good purpose as a fuel, it creates certain problems which cannot be overlooked. Any type of coal will have a certain percentage of ash. Ash may be a potential pollutant which is not desired.

The coal on being burned with the oxidizer will produce various gases such as water vapor, carbon dioxide, carbon monoxide, sulfur dioxide, and slag in gaseous form or liquid droplets or solid particles. The seeding agent introduced is potassium carbonate. The slag contains silica, oxides, silicates, sulfides and other compounds. A typical coal analysis [4] after pulverizing is outlined in Table 1 and the ash analysis [4] in Table 2.

Table 1. Typical Coal Composition [4]

Components	Percentage	
Moisture	3.0	±1.0
Ash	12.5	±2.5
Sulfur	3.9	±0.2
Carbon	66.0	±3.0
Hydrogen	4.9	±0.2
Nitrogen	1.2	±0.1
Oxygen	8.5 (by difference)	
Joules/kg (HHV)	28×10^6	3.5×10^5

Table 2. Ash Analysis (Percent in Ash) [4]

Constituents	Percentage	
SiO_2	53.0	±3.0
Al_2O_3	14.0	±2.0
Fe_2O_3	21.0	±2.5
CaO	3.9	±0.5
K_2O	2.3	±0.3
Na_2O	0.3	±0.1
TiO_2	0.9	±0.1
MgO	0.9	±0.1

Pollutants being a potential health hazard, it is desired that particulates be removed from the gaseous stream. At the prevailing temperature in the different components of the MHD plant, the particulates may be in the form of liquid droplets in the gaseous stream or may condense from vapor phase to liquid phase in the gaseous stream. As expected, it is easier to remove large particles as compared to the finer ones. To remove fine particulates, sophisticated and, hence, costly types of equipment are needed [5]. In order to facilitate efficient removal, it is desirable that fine particles either agglomerate or migrate to the wall and hence be removed in this way.

CHAPTER II

MECHANISMS OF AGGLOMERATION

There are many factors that may affect agglomeration; namely, turbulence, impaction, interception, thermophoresis, and Brownian diffusion.

In impaction, the center of mass of one particle crosses streamlines so that the extension of its path is blocked by the particle on which it is impacting. In interception, the center of mass of the first particle may bypass the second particle, but because of the physical size of the first particle, a grazing impaction or "interception" occurs.

If one considers that in turbulence, all particles oscillate to a certain degree, then the chances of particles either undergoing impaction or interception may or may not be small. In Appendix B, an estimate is made that about 2 percent of the fine particles may be collected due to turbulence in the apparatus here, and hence, impaction and interception phenomena are not discussed further.

Thus, for the problem under consideration, Brownian diffusion and thermophoresis shall be discussed.

Brownian Diffusion

An equation is derived in order to obtain the relative accretion rate of fine particles onto large particles due to diffusion.

Depending on the value thus obtained, the significance of Brownian diffusion shall be discussed.

Define mass flux of fine particles to a large particle as

$$\vec{n}_A = - \mathcal{D} \rho_g \nabla \omega_A \ . \tag{2.1}$$

For coordinate R (distance from center of a collecting particle), Eq. (2.1) reduces to

$$n_{AR} = - \mathcal{D} \rho_g \frac{\partial \omega_A}{\partial R} \ . \tag{2.2}$$

Assume mass flow to a large particle as constant,

$$\dot{m}_{AR} = - 4\pi R^2 \mathcal{D} \rho_g \frac{\partial \omega_A}{\partial R} \ . \tag{2.3}$$

As $R \to \infty$,

$$\omega_A = \omega_{A_\infty} \ ; \tag{2.4}$$

at $R = r_{bp}$,

$$\omega_A = 0.0 \ .$$

Integrating Eq. (2.3) for conditions specified in Eq. (2.4),

$$- \dot{m}_{AR} = 4\pi \mathcal{D} \rho_g \ \omega_{A_\infty} \ r_{bp} \ . \tag{2.5}$$

The diffusion coefficient [6] due to Brownian motion of the particle is

$$\mathcal{D} = k \ T_g \ B \ , \tag{2.6}$$

and mobility [7] of the particle is

$$B = \frac{1.0 + \frac{\lambda}{r_{sp}}\left(A' + B' e^{-C' \frac{r_{sp}}{\lambda}}\right)}{6\pi\mu_g r_{sp}} , \tag{2.7}$$

where

$$A' = 1.2 ,$$

$$B' = 0.41 ,$$

$$C' = 0.88 .$$

The constants A', B', and C' are found experimentally when the mean free path λ is defined as

$$\lambda = \frac{\mu_g}{0.499\ \rho_g\ \bar{u}_g} . \tag{2.8}$$

Relative accretion rate on a large particle is given by $-\dot{m}_{AR}/m_p$:

$$-\frac{\dot{m}_{AR}}{m_p} = \frac{4\pi\ r_{bp}\ \mathcal{D}\rho_g\ \omega_{A_\infty}}{\frac{4}{3}\pi r_{bp}^3\ \rho_p} , \tag{2.9}$$

$$-\frac{\dot{m}_{AR}}{m_p} = \frac{3\ \omega_{A_\infty}\ \mathcal{D}}{r_{bp}^2} \cdot \frac{\rho_g}{\rho_p} . \tag{2.10}$$

When evaluated, Eq. (2.10) will give the relative accretion rate on a large particle.

Thermophoresis

Thermophoresis is a phenomenon in which particles suspended in a gas in which there exists a temperature gradient ∇T, will experience a force in the direction opposite to that of ∇T. A common example is the blackening of the glass globe of a kerosene lantern by soot particles from the hot flame migrating to the cool glass.

Maxwell was the first to investigate the phenomenon of thermophoresis in an attempt to explain the radiometer effect. Radiometric forces depend essentially on the ratio of the particle radius to the mean free path of the gas molecules.

According to Fuchs [6], for $r << \lambda$, thermophoresis is due to the gas molecules impinging on the particle from opposite sides with different mean velocities.

For $r >> \lambda$, this mechanism is more complicated. Consider an unequally heated solid boundary in contact with a gas. The layer of gas adjacent to the wall will have approximately the same tangential gradient. The gas molecules from the hotter region will impinge on an elemental surface ds with a higher average velocity than those coming from the colder region, because of which an unequal tangential momentum is delivered. Thus, a shear stress is exerted by the gas on the wall in a direction opposite to the temperature gradient parallel to the wall in the gas.

Suitable equations are chosen in order to define thermophoretic forces and thermophoretic velocity for the fine particles agglomerating on large particles.

Table 3 [8] gives various expressions for thermal forces, their range of applicability and limitations. These expressions are not general in the sense that they cannot be applied to the entire range of Knudsen number (defined as the ratio of mean free path of the gas and the radius of the particle) and hence, it is desirable to have an expression that can be applied to the entire range of Knudsen number. One way of obtaining this is to construct an interpolation formula which matches the theory in the near-continuum and free molecular (collisionless) limits.

For collisionless limits, as stated by Talbot et al. [7], Waldmann proposed

$$\lim_{\frac{\lambda}{r} \to \infty} F_t \equiv F_{t_\infty} = - 2\pi\nu \frac{r^2}{\lambda} \frac{\nabla T}{T_o} \mu_g \ , \tag{2.11}$$

and for the near-continuum limit, Brock [9] proposed

$$F_t = - \frac{12\pi\mu_g \nu r C_s \left(\frac{k_g}{k_p} + C_t \frac{\lambda}{r} \right) \frac{T}{T_o}}{\left(1 + 3C_m \frac{\lambda}{r} \right) \left(1 + 2\frac{k_g}{k_p} + 2C_t \frac{\lambda}{r} \right)} \ . \tag{2.12}$$

When $\lambda/r \to \infty$, Eq. (2.12) reduces to Eq. (2.11), except for the factor $C_s/C_m = 1.17/1.14 = 1.03$ and hence, only 3 percent deviation is introduced by using Eq. (2.11), as pointed out by Talbot et al. [7].

Brock's equation is an improvement over Epstein's equation (see Table 3). Brock carried out a hydrodynamic analysis based on Navier-Stokes-Fourier theory with slip corrected boundary conditions

Table 3. Expressions for Thermal Force [8]

Investigator	Thermal Force Expression	Range of Applicability	Comments
Cawood	$F_t = -\frac{1}{2}\pi r^2 p \frac{\lambda}{T}\frac{dT}{dx}$	$\frac{\lambda}{r} >> 1$	Underestimates thermal force by approximately a factor of $8/\pi$.
Waldmann, Derjaguin, and Bakanov	$F_t = -4r^2 p \frac{\lambda}{T}\frac{dT}{dx}$	$\frac{\lambda}{r} >> 1$	Shows good agreement with experimental results.
Epstein	$F_t = -9\pi r \frac{\mu_g^2}{\rho_g T}\left(\frac{k_g}{2k_g + k_p}\right)\frac{dT}{dx}$	$\frac{\lambda}{r} << 1$ Continuum Regime	Not applicable for particles of high thermal conductivity.
Brock	$F_t = -\frac{12\pi(\mu_g r)\nu C_s\left(\frac{k_g}{k_p} + C_t\frac{\lambda}{r}\right)\frac{\nabla T}{T_o}}{\left(1 + 3C_m\frac{\lambda}{r}\right)\left(1 + 2\frac{k_g}{k_p} + C_t\frac{\lambda}{r}\right)}$	$\frac{\lambda}{r} < 1$	Shows good agreement with experimental results.
Derjaguin and Yalamov	$F_t = -\frac{3\pi\mu_g^2 r}{\rho_g T}\left[\frac{8k_g + k_p + 2C_t k_p\frac{\lambda}{r}}{2k_g + k_p + 2C_t k_p\frac{\lambda}{r}}\right]\frac{dT}{dx}$	$\frac{\lambda}{r} << 1$	Overestimates thermal force by about 20%; shows no dependency of force on size of particle.
Brock	$F_t = F_t^* \exp(-\tau r/\lambda)$	$\frac{\lambda}{r} \simeq 1$ Transition Regime	Derived for monatomic gases; only a qualitative estimate of thermal force for polyatomic gases.

to obtain Eq. (2.12). A full description of this is given by Talbot et al. [7].

The term C_t is defined as the temperature jump coefficient, C_m as the momentum exchange coefficient, and C_s as the thermal slip coefficient. The terms C_t, C_m, and C_s are numerical factors of order unity and these are obtained from kinetic theory.

Assuming that there are only thermophoretic and drag forces, the thermophoretic velocity U_T for the entire range of Knudsen number is obtained by equating thermophoretic force to the Millikan drag formula [7], F_v.

$$F_t = -F_v \ , \tag{2.13}$$

$$\frac{-12\pi\mu_g \nu r C_s\left(\frac{k_g}{k_p}+C_t\frac{\lambda}{r}\right)\frac{\nabla T}{T_o}}{\left(1+C_m\frac{\lambda}{r}\right)\left(1+2\frac{k_g}{k_p}+2C_t\frac{\lambda}{r}\right)} = \frac{6\pi\mu_g U_T r}{1+\frac{\lambda}{r}\left(A'+B'e^{-C'\frac{r}{\lambda}}\right)} \ . \tag{2.14}$$

The above relation simplifies to give thermophoretic velocity [7]

$$U_T = \frac{-2C_s\nu\left(\frac{k_g}{k_p}+C_t\frac{\lambda}{r}\right)\left[1+\frac{\lambda}{r}\left(A'+B'e^{-C'\frac{r}{\lambda}}\right)\right]\frac{\nabla T}{T_o}}{\left(1+3C_m\frac{\lambda}{r}\right)\left(1+2\frac{k_g}{k_p}+2C_t\frac{\lambda}{r}\right)} \ , \tag{2.15}$$

where

$$A' = 1.2 \ ,$$

$$B' = 0.41 \ ,$$

$$C' = 0.88 \ ,$$

$$C_m = 1.14 \ ,$$

$$C_s = 1.17 ,$$

$$C_t = 2.18 .$$

The mean free path of the gas is calculated by Eq. (2.8). This relation for the mean free path has been used by Talbot et al. [7] to obtain the numerical coefficients C_s, C_m, and C_t.

Mean molecular velocity is defined as

$$\bar{u}_g = \sqrt{\frac{8 k T_g}{\pi M_g}} . \tag{2.16}$$

CHAPTER III

METHODS AND PROCEDURES

Thermophoresis of Fine Particles to the Large Particles

The driving force for thermophoresis is the temperature difference between the large particles and the gas due to convection between gas and large particles, and radiation between large particles and the wall of the tubes. The fine particles, however, have negligible temperature difference from gas. The particles are considered to be spherical in shape.

Temperature Gradient

In order to calculate the thermophoretic velocity of fine particles moving towards large particles, an expression for $\nabla T/T_o$ is needed in Eq. (2.15). This is obtained as follows, leading to Eq. (3.9) using Eqs. (3.11) and (3.13).

$$\text{Convective heat flux} = \dot{q}'' = h\,(T_g - T_p)\,, \tag{3.1}$$

$$\text{Conduction heat flux} = \dot{q}'' = -k_g \left.\frac{dT}{dR}\right|_{\substack{\text{surface of}\\ \text{large particle}}}. \tag{3.2}$$

Both Eq. (3.1) and Eq. (3.2) are two different ways of expressing the same thing, and hence, on equating both these equations and rearranging,

$$\left.\frac{dT}{dR}\right|_{\substack{\text{surface of}\\ \text{large particle}}} = -\,(T_g - T_p)\,\frac{h}{k_g}\,. \tag{3.3}$$

In relative motion between a sphere and fluid [10], for $Pr = 0.7$,

$$Nu = 2.0 + 0.6\, Re_v^{0.5}\, Pr^{1/3} \quad , \quad 0 \leq Re_v \leq 10^5 \ . \tag{3.4}$$

The Reynolds number based on velocity difference of particle and gas in turbulent fluctuations is very small, as shown in Appendix C. Hence, Eq. (3.4) can be approximated by

$$Nu = 2.0 \ , \tag{3.5}$$

$$\frac{hD_{bp}}{k_g} = 2.0 \ , \tag{3.6}$$

$$h = k_g / r_{bp} \ . \tag{3.7}$$

Substituting for h in Eq. (3,3),

$$\left.\frac{dT}{dR}\right|_{\substack{\text{surface of} \\ \text{large particle}}} = - \frac{T_g - T_p}{r_{bp}} \ . \tag{3.8}$$

The term T_o represents the mean temperature in the vicinity of the particle and this can be taken to be gas temperature, T_g. Thus,

$$\frac{\nabla T}{T_o} = \frac{\nabla T}{T_g} = - \frac{T_g - T_p}{r_{bp}} \cdot \frac{1}{T_g} \ . \tag{3.9}$$

This value of $\nabla T/T_o$ applies at the surface of the particle.

The temperature of the particle, T_p, is obtained by equating

$$\text{radiation heat flux} = \dot{q}'' = \varepsilon\sigma\,(T_p^4 - T_w^4) \tag{3.10}$$

and convective heat flux, Eq. (3.1). This rearranges to

$$T_g - T_p = \frac{\varepsilon\sigma}{h}(T_p^4 - T_w^4)\,. \tag{3.11}$$

From ash analysis, particles consist mainly of silica. For the range of temperature of interest here, the emissivity of silica [11] varies from ~0.75 to ~0.84; hence, 0.8 is a suitable approximation for emissivity.

Wall temperature, T_w, is obtained using the following relation:

$$\dot{q}'' = \frac{k_m}{\ell_w}\,(T_w - T_{water})\,, \tag{3.12}$$

assuming the heat transfer coefficient of water is high. Heat loss $\dot{q}''$ is known for each component [12]. Water is used to cool the system.

Equation (3.12) can be rewritten as

$$T_w = T_{water} + \dot{q}''\,\frac{\ell_w}{k_m}\,. \tag{3.13}$$

When T_w is known, T_p may be calculated by a trial and error procedure from Eq. (3.11).

Flow Time

In order to calculate collection efficiency, η, it is necessary to calculate flow time, t. Flow time t depends on mass flow

rate, $\dot{m}$

$$dt = \frac{dx}{\bar{V}} , \tag{3.14}$$

$$t = \int \frac{dx}{\bar{V}} . \tag{3.15}$$

But,

$$\bar{V} = \frac{\dot{m}}{A\rho_g} , \quad \rho_g = \frac{pM_g}{R'T_g} . \tag{3.16}$$

Equation (3.15) reduces to

$$t = \frac{pM_g}{R'} \frac{A}{\dot{m}} \int \frac{dx}{T} . \tag{3.17}$$

For the diffuser, an average value of A is assumed.

Assume a linear profile for temperature in each component. (This assumption, which implies a constant heat flux is not more than about 1 percent in error compared with a more sophisticated calculation, even for the component of largest temperature drop, is shown in Appendix D).

$$T = a + bx , \tag{3.18}$$

where

$$b = (T_{g2} - T_{g1}) / L , \tag{3.19}$$

$$a = T_{g1} . \tag{3.20}$$

Then Eq. (3.17) reduces to

$$t = \frac{pM_g}{R'} \frac{A}{\dot{m}} \frac{1}{b} \ln \frac{a + bx_2}{a + bx_1} , \tag{3.21}$$

$$t = \frac{pM_g}{R'} \frac{A}{\dot{m}} \frac{1}{b} \ln \frac{T_{g2}}{T_{g1}} . \tag{3.22}$$

Collection Efficiency

Collection efficiency, η, is derived in the following way to obtain Eq. (3.37) using Eqs. (3.34) and (3.41):

$$\text{velocity, } u = \frac{dR}{dt} , \tag{3.23}$$

$$\frac{dR}{dt} = -U_T \frac{r_{bp}^2}{R^2} , \tag{3.24}$$

$$-\frac{1}{3} \frac{d}{dt}(R^3) = U_T r_{bp}^2 . \tag{3.25}$$

Equation (3.24) is derived in Appendix E.

Assume that a fine particle at a distance R_1 from a large particle in the first component will be at a distance R_2 in the second component, R_3 in the third component, and so on, and finally at R_8 in the eighth component. Any fine particle at a distance R_8 or within that range will be collected by the large particle in the eighth component.

Then on integrating Eq. (3.25) for the

$$\text{eighth component: } \left(\frac{R_8}{r_{bp}}\right)^3 - 1.0 = \left.\frac{3U_T t}{r_{bp}}\right|_8 , \tag{3.26}$$

$$\text{seventh component: } \left(\frac{R_7}{r_{bp}}\right)^3 - \left(\frac{R_8}{r_{bp}}\right)^3 = \left.\frac{3U_T t}{r_{bp}}\right|_7 , \tag{3.27}$$

sixth component: $$\left(\frac{R_6}{r_{bp}}\right)^3 - \left(\frac{R_7}{r_{bp}}\right)^3 = \left.\frac{3U_T t}{r_{bp}}\right|_6 , \qquad (3.28)$$

fifth component: $$\left(\frac{R_5}{r_{bp}}\right)^3 - \left(\frac{R_6}{r_{bp}}\right)^3 = \left.\frac{3U_T t}{r_{bp}}\right|_5 , \qquad (3.29)$$

fourth component: $$\left(\frac{R_4}{r_{bp}}\right)^3 - \left(\frac{R_5}{r_{bp}}\right)^3 = \left.\frac{3U_T t}{r_{bp}}\right|_4 , \qquad (3.30)$$

third component: $$\left(\frac{R_3}{r_{bp}}\right)^3 - \left(\frac{R_4}{r_{bp}}\right)^3 = \left.\frac{3U_T t}{r_{bp}}\right|_3 , \qquad (3.31)$$

second component: $$\left(\frac{R_2}{r_{bp}}\right)^3 - \left(\frac{R_3}{r_{bp}}\right)^3 = \left.\frac{3U_T t}{r_{bp}}\right|_2 , \qquad (3.32)$$

first component: $$\left(\frac{R_1}{r_{bp}}\right)^3 - \left(\frac{R_2}{r_{bp}}\right)^3 = \left.\frac{3U_T t}{r_{bp}}\right|_1 . \qquad (3.33)$$

On summing from Eq. (3.26) to Eq. (3.33),

$$\left(\frac{R_1}{r_{bp}}\right)^3 - 1.0 = \frac{3}{r_{bp}} \sum U_T t . \qquad (3.34)$$

In any component, as for example, the third component, the left-hand side of Eq. (3.31) represents the volume within which any fine particle will be a distance R_8 from a large particle at the entrance of the eighth component.

Let the large particles be at a configuration such that their centers are at a distance ℓ apart. Then the collection efficiency for any large particle is given by

$$\eta = \frac{\text{relative volume cleared of small particles}}{\text{volume occupied by one large particle}} , \tag{3.35}$$

$$\eta = \frac{\frac{4}{3}\pi \left(R_1^3 - r_{bp}^3 \right)}{\ell^3} , \tag{3.36}$$

$$\eta = \frac{\frac{4}{3}\pi \left[\left(\frac{R_1}{r_{bp}} \right)^3 - 1.0 \right]}{\left(\frac{\ell}{r_{bp}} \right)^3} . \tag{3.37}$$

Within a cubic volume ℓ^3,

$$m_p = \frac{4}{3} \rho_p r_{bp}^3 \pi , \tag{3.38}$$

$$m_g = \ell^3 \rho_g , \tag{3.39}$$

m_p/m_g can be approximated by 0.04 (Appendix F). Then,

$$0.04 = \frac{\frac{4}{3} \pi r_{bp}^3 \rho_p}{\ell^3 \rho_g} , \tag{3.40}$$

$$\left(\frac{\ell}{r_{bp}} \right)^3 = \frac{4}{3} * \frac{\pi}{0.04} * \frac{\rho_p}{\rho_g} . \tag{3.41}$$

Method of Application to a Distribution of Particle Sizes

The model described in the preceding sections has been applied to the distribution calculated by Im et al. [2]. For Im's model, total mass fraction of fine particles is 0.36 and hence, total mass fraction of large particles is 1.0 - 0.36 = 0.64. Between any range of large particles' radii, $r_i \pm \Delta r$, if the mass fraction is ω_A', then the

relative mass fraction of large particles will be $\omega_A'/0.64$. This relative mass fraction of large particles should be capable of interacting with $\omega_A'/0.64$ of fine particles. Then, overall mass fraction of fine particles collected will be

$$\left(\frac{\omega_A'}{0.64}\right) (0.36)\ \eta_i \ .$$

Similar calculations are carried out for a suitable range of large particles, and on adding the contributions from all the large particles, the sum will tell what fraction of fine particles is collected. Since most of the fine particles (Figure 1, page 2) are near radius 0.05 μm and 0.1 μm, an average η_i obtained for these fine particles has been used.

The amount of fine particles collected by large particles is added to the mass fraction of the large particles and subtracted from the mass fraction of the fine particles. This will give a plot for the present model as presented in Chapter IV. Values and calculations are shown in Appendix G.

Fine particles agglomerating on large particles will increase the size of the large particles.

$$\text{Number of particles per unit mass} = N_A = \frac{\omega_A'}{\frac{4}{3}\pi r_i^2 \rho_p} , \qquad (3.42)$$

$$\text{Relative increase in mass fraction} = \delta\omega_A' = 0.36\ \eta_i \ . \qquad (3.43)$$

The number of particles remains the same.

Thus, increase in radius is given by

$$\frac{\delta r_i}{r_i} = -1 + \left(1 + \frac{0.36}{0.64}\,\eta_i\right)^{1/3} . \qquad (3.44)$$

Values for this have been noted in Appendix G.

Migration of Fine Particles to the Wall

Deposition of particles on a surface is caused by different mechanisms largely depending on particle size, as discussed by Im and Chung [13].

Particles, by virtue of fluid turbulence, will diffuse across the mean streamlines toward the wall. The momentum of fine particles dissipates in the laminar sublayer, and turbulence alone does not suffice to cause the particles to diffuse to the wall. At this stage, thermophoresis is an effective phenomenon which will continue the particulate migration to the wall.

Particles of a diameter of several micrometers have sufficient momentum to be able to cross the laminar sublayer and deposit on the wall.

The velocity profile in turbulent flow can be divided into three regions [13]: fully turbulent, buffer layer, and laminar sublayer (Figure 3).

Effective Deposition Velocity

According to Im and Chung [13], effective deposition velocity of any particle originating in the fully turbulent region with a mass fraction C_A is given by

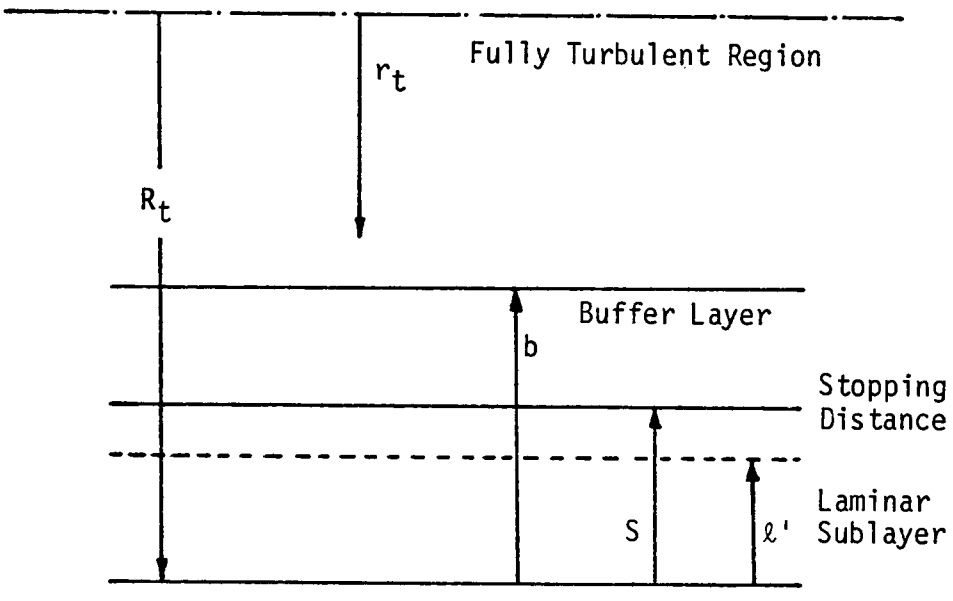

Figure 3. Sketch of flow regions.

$$\frac{J}{C_A} = \frac{1}{\frac{1}{\hat{D}(b)} + \frac{1}{V}} , \tag{3.45}$$

where J is the particle flux toward the surface, $\hat{D}(b)$ is the effective diffusion velocity of the particles across the buffer layer, and V is related to their migration velocity through the sublayer adjacent to the wall; V is controlled by either turbulence-imparted momentum or thermophoresis. Calculations have been performed and it is seen that the turbulence-imparted momentum does not have any significant effect for particles whose radius varies from 0.086 to 0.86 μm and hence, it can be totally neglected.

Effective Turbulent Diffusion Velocity

The term $\hat{D}(b)$ is defined as

$$\hat{D}(b) = \left[\int_s^b \frac{dy}{\mathcal{D}_e}\right]^{-1} = \frac{0.4\ V^*}{Sc\left\{0.92\ \ell n\left(\frac{b^+}{S^+ + k_s^+}\right) + \frac{13}{S^+ + k_s^+} + \frac{365}{\left(S^+ + k_s^+\right)^2}\right\}} , \tag{3.46}$$

where

$$b^+ = b\,\frac{V^*}{\nu} ,$$

$$S^+ = S\,\frac{V^*}{\nu}$$

$$k_s^+ = k_s\,\frac{V^*}{\nu} .$$

The particulate Schmidt number is

$$Sc = \frac{\varepsilon'}{\mathcal{D}_e} , \tag{3.47}$$

where

ε' = eddy diffusivity of gas ,

$\mathcal{D}_e$ = particulate eddy diffusivity .

For fine particles, as shown in Ref. [13],

$$\frac{\mathcal{D}_e}{\varepsilon'} \to 1 \ ;$$

hence,

$$Sc^{-1} \to 1 \ ;$$

thus,

$$Sc = 1.0 \ .$$

Assuming hydrodynamically smooth surface, surface roughness,

$$k_s = 0.0 \ ;$$

thus,

$$k_s^+ = 0.0 \ .$$

The buffer layer region [14] exists between b^+ and ℓ^+. Reasonable values for these are

$$b^+ = 30.0 \ ,$$

$$\ell^+ = 6.0 = S^+ \ .$$

If turbulent deposition is effective, $S \geq \ell'$, but if it is not, and thermophoresis is, then replace S with ℓ'.

Friction velocity V^* is obtained from the following relation:

$$\frac{V^*}{\nu} = \frac{V^*}{\bar{V}} \cdot \frac{\bar{V}}{\nu} , \tag{3.48}$$

$$\frac{V^*}{\bar{V}} = \sqrt{\frac{f}{2}} , \tag{3.49}$$

$$\frac{\bar{V}}{\nu} = \frac{Re}{D} . \tag{3.50}$$

For $3x10^4 < Re < 10^6$, the friction coefficient factor [15] is

$$\frac{f}{2} = 0.023\ Re^{-0.2} . \tag{3.51}$$

Equation (3.49) reduces to

$$V^* = \bar{V}\left(0.023\ Re^{-0.2}\right)^{1/2} \tag{3.52}$$

and Eq. (3.46) simplifies to

$$\hat{D}(b) = \frac{0.4\ \bar{V}\left(0.023\ Re^{-0.2}\right)^{1/2}}{0.92\ \ell n\ \frac{30.0}{6,0} + \frac{13.0}{6.0} + \frac{365}{(6.0)^2}} . \tag{3.53}$$

Steady-state velocity, $\bar{V}$, is obtained from

$$\bar{V} = \frac{\dot{m}}{\rho_g A} , \tag{3.54}$$

$$\bar{V} = \frac{\dot{m}}{\rho_g \left(\frac{\pi D^2}{4}\right)} . \tag{3.55}$$

Thus, $\hat{D}(b)$ is calculated using Eq. (3.53), but to obtain J/C_A, a value for V is still required.

Particle Diffusion Velocity

Conduction heat flux from the gas to the surface of the tube is equal to the convective heat flux,

$$k_g \nabla T = h (T_g - T_w) . \tag{3.56}$$

Applying Reynolds analogy,

$$St = \frac{f}{2} = \frac{h}{\rho_g \overline{V} C_p} . \tag{3.57}$$

$$\nabla T = \frac{\overline{V}}{\alpha} \cdot \frac{f}{2} \cdot (T_g - T_w) , \tag{3.58}$$

which is the temperature gradient at the surface, and this gradient will be constant through the laminar sublayer.

If in Eq. (2.15), the equation is rearranged to read

$$\frac{U_T T_o}{\nu \nabla T} = A2 (Kn) , \tag{3.59}$$

where

$$A2 = \frac{- 2C_s \left(\frac{k_g}{k_p} + C_t \frac{\lambda}{r} \right) \left[1 + \frac{\lambda}{r} \left(A' + B' \, e^{-C' \frac{r}{\lambda}} \right) \right]}{\left(1 + 3C_m \frac{\lambda}{r} \right) \left(1 + \frac{2k_g}{k_p} + 2C_t \frac{\lambda}{r} \right)} ;$$

then,

$$U_T = A2 \cdot \frac{\overline{V}}{\alpha} \cdot \nu \cdot \frac{f}{2} \cdot \frac{T_g - T_w}{T_w} , \tag{3.60}$$

$$U_T = A2 \cdot \overline{V} \cdot Pr \cdot \left(0.023\ Re^{-0.2} \right) \frac{T_g - T_w}{T_w} , \tag{3.61}$$

where, for this region, $T_o \approx T_w$. Thus, $U_T = V$ is the effective diffusion velocity of the particles across the laminar sublayer. The terms $\hat{D}(b)$ and V being known, J/C_A is calculated using Eq. (3.45) and hence, collection efficiency, ψ.

Collection Efficiency

Collection efficiency is defined as

$$\psi = 1 - \frac{C_A}{C_{A_0}} , \tag{3.62}$$

$$\frac{C_A}{C_{A_0}} = \exp\left[- \frac{J}{C_A} \cdot \frac{4}{\overline{V}} \cdot \frac{L}{D} \right] , \tag{3.63}$$

$$\psi = 1 - \exp\left[- \frac{J}{C_A} \cdot \frac{4}{\overline{V}} \cdot \frac{L}{D} \right] . \tag{3.64}$$

Equation (3.63) is derived in Appendix H.

Collection efficiency ψ_{TOT} is obtained as follows:

$$\left(\frac{C_{AOUT}}{C_{AIN}}\right)_1 \left(\frac{C_{AOUT}}{C_{AIN}}\right)_2 \left(\frac{C_{AOUT}}{C_{AIN}}\right)_3 \left(\frac{C_{AOUT}}{C_{AIN}}\right)_4 \left(\frac{C_{AOUT}}{C_{AIN}}\right)_5$$

$$\left(\frac{C_{AOUT}}{C_{AIN}}\right)_6 \left(\frac{C_{AOUT}}{C_{AIN}}\right)_7 \left(\frac{C_{AOUT}}{C_{AIN}}\right)_8 = \frac{(C_{AOUT})_8}{(C_{AIN})_1} , \tag{3.65}$$

$$C_{AOUT})_i = (C_{AIN})_{i+1} \quad , \; i = 1,2,3,\ldots,7 \tag{3.66}$$

$$\psi_{TOT} = 1 - \frac{(C_{AOUT})_8}{(C_{AIN})_1} \quad . \tag{3.67}$$

A subscript outside the parentheses indicates the component numbers.

CHAPTER IV

RESULTS AND DISCUSSION

Brownian Motion Contribution to Fine Particle Collection on Large Particles

For a typical condition:

$$\omega_{A_\infty} = 0.01 \ ,$$

$$r_{bp} = 1.0 \ \mu m \ ,$$

$$\rho_g = 1.5 \times 10^{-4} \ gm \ cm^{-3} \ ,$$

$$\rho_p = 2.5 \ gm \ cm^{-3} \ ,$$

$$T_g = 2{,}300^{o}K \ ,$$

$$p = 1 \ atm \ ,$$

$$\mu_g = 6.0 \times 10^{-4} \ gm \ cm^{-1} \ sec^{-1} \ ,$$

$$\lambda = 0.575 \ \mu m \ ,$$

$$r_{sp} = 0.1 \ \mu m \ ,$$

from Eq. (2.6),

$$\mathcal{D} = 2.78 \times 10^{-5} \ cm^2/sec \ ,$$

and from Eq. (2.10),

$$-\frac{\dot{m}_{AR}}{\dot{m}_p} = 5.00 \times 10^{-3} \ gm/sec/gm \ ,$$

which is a very small quantity and hence, Brownian diffusion can be neglected.

For r_{bp} = 10 μm,

$$-\frac{\dot{m}_{AR}}{m_p} = 5.00\text{x}10^{-5} \text{ gm/sec/gm} ,$$

which is still a very small quantity.

Thermophoresis Calculations

A computer program has been developed in order to solve various equations needed to obtain the desired output values.

Table 4 indicates the values of input variables in the different components of the MHD plant that have been used for obtaining the desired results. These various components for which calculations have been carried out are shown in Figure 4 [16]. The samples were taken at the sampling section.

Since major components of flue gases are oxygen, carbon dioxide, water vapor, nitrogen, hydrogen, and carbon dioxide, and since their average mean free path is similar to that of air, properties of air have been considered for the purpose of calculation [11]. Also, an average value of gas temperature has been assumed in each component for thermophoresis calculations. The average value is obtained using the inlet and outlet temperatures in each component.

The total mass flow rate is 1.7 lb/sec and the temperature of the cooling water is 60.0°F.

Input variables such as temperature, molecular weight, specific heat, and density have been obtained by running the UTSI version of the NASA-LEWIS program [17]. Percentage of heat loss at each

Table 4. Input Data

	Component Number								
	0	1	2	3	4	5	6	7	8
Component Description	Segmented Conductivity Channel	Diffuser	Cyclone	Exhaust Stack	Reducer	Straight Section	Elbow	Straight Section	Sampling Section
Material of Construction	---	Stainless Steel(SS)	SS	SS	Carbon Steel(CS)	CS	CS	CS	CS
Internal Diameter $x10^2$, m	---	35.56	72.72	49.23	49.23	38.735	38.735	38.735	38.735
Wall Thickness $x10^2$, m	---	0.4826	0.9525	0.9525	0.9525	0.9525	0.9525	0.9525	0.9525
Length $x10^2$, m	---	118.75	125.73	158.75	52.71	59.69	52.55	99.21	45.72
Thermal Conductivity of Material, watts/m-^oK	---	5.782	5.782	5.782	17.345	17.345	17.345	17.345	17.345
Average Temperature, ^oK	---	2,215.0	1,960.0	1,588.6	1,305.2	1,221.9	1,155.2	1,094.1	1,044.1
Outlet Temperature, ^oK	2,340.0	2,090.0	1,824.7	1,349.7	1,255.2	1,188.6	1,127.4	1,060.8	1,021.9

Table 4. (continued)

	Component Number								
	0	1	2	3	4	5	6	7	8
Molecular Weight	---	31.646	32.022	32.362	32.572	32.599	32.609	32.611	32.613
Prandtl No.	---	0.7650	0.7650	0.7610	0.7500	0.7457	0.7424	0.7393	0.7349
Viscosity $x10^5$, kg/m-sec	---	6.40	6.01	5.42	4.99	4.79	4.63	4.48	4.35
Thermal Conductivity of Gas, watts/m-^oK	---	0.03429	0.03225	0.02904	0.02633	0.02511	0.02411	0.02321	0.02238
Mean-Free Path $x10^6$,m	---	0.63874	0.56522	0.45812	0.37922	0.35122	0.32323	0.31050	0.29523
Density, kg-m^{-3}	---	0.17421	0.19948	0.24649	0.30719	0.32587	0.34607	0.36630	0.38288
Heat Flux $x10^{+4}$, watts/m^2	---	19.67	8.10	32.67	13.02	10.25	8.32	8.30	8.28
Specific Heat kJ/kg-^oK	---	0.10361	0.10892	0.09823	0.09315	0.08748	0.08595	0.08604	0.08612

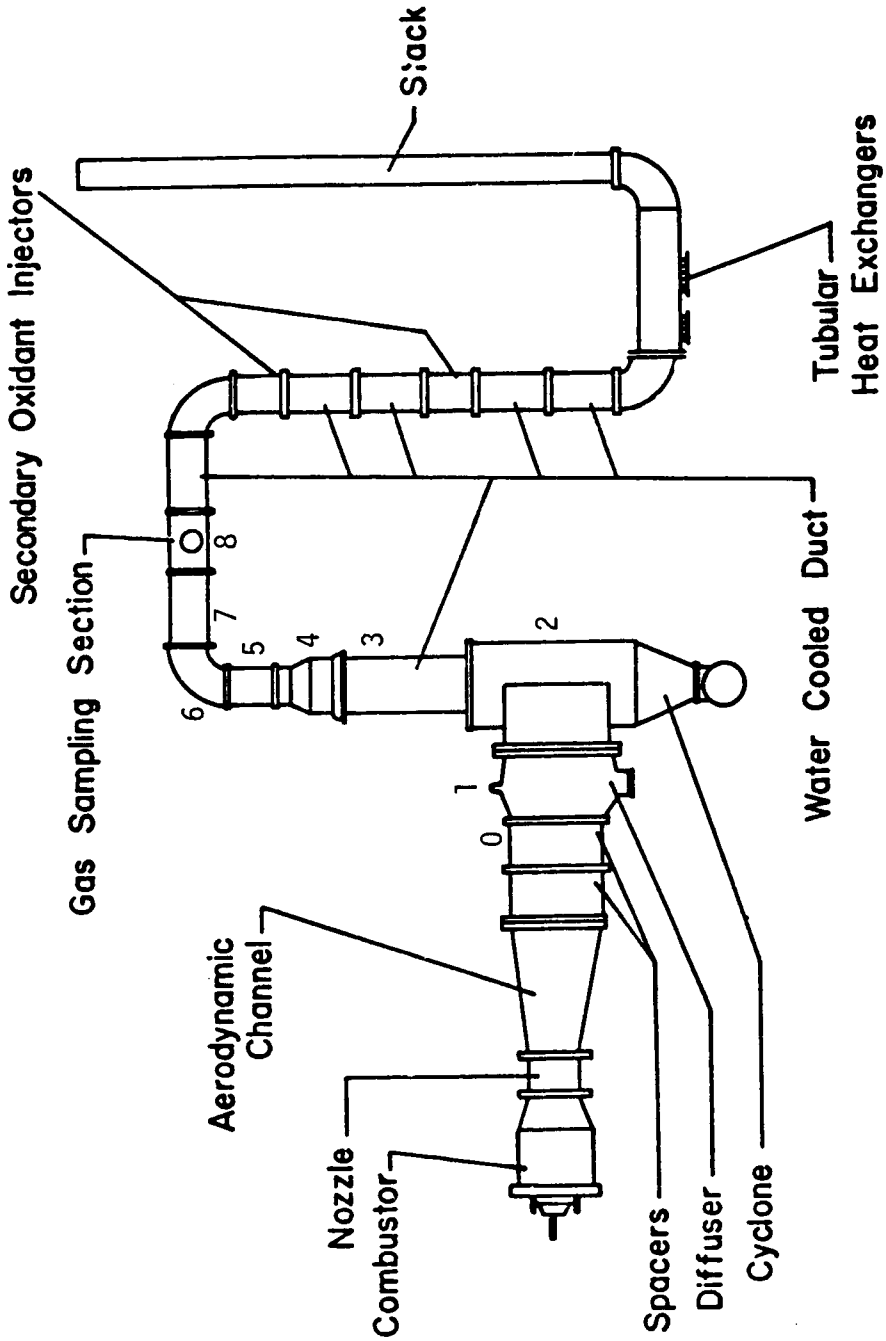

Figure 4. Cell III downstream test facility.

temperature has been calculated, and knowing the percentage of heat loss in each component [14], temperature, molecular weight, specific heat, and density are found by interpolation. Other variables such as Prandtl number, viscosity, and thermal conductivity have been obtained from tables given by Kreith [11].

Variables such as wall and particle temperature, mean molecular and thermophoresis velocity, and flow time for a particle have been calculated in order to obtain collection efficiency η and ψ_{TOT}. These values have been noted in Tables 5, 6, and 7.

The fine particle sizes (radius) studied are 0.01, 0.02, 0.05, 0.1, 0.2, and 0.5 μm, and the large particle sizes (radius) are 1.5 and 5.0 μm. Other large particle sizes (radius) between 1.5 and 5.0 μm have been studied but their values are not reported.

As seen from the results, the particle temperature decreases with increase in the radius of the large particle. This is expected because of the higher heat transfer coefficient for the smaller particles.

Mean molecular velocity in each component remains constant as it is independent of particle radius and depends on temperature and molecular weight. Thermophoresis velocity decreases with decrease in Knudsen number and increase in large particle radius (see Table 7). Flow time is made constant for each component (see Table 5).

The collection efficiency η is an overall collection efficiency which decreases with increase in large particle radius (Figure 5). The symbol η represents collection efficiency for fine particles agglomerating with the large particles (Table 6). For a large

Table 5. Output Values

Component No.	Reynolds No., $\times 10^{-5}$	Wall Temperature, ^{o}K	Particle Temperature (for 1.5 μm), ^{o}K	Particle Temperature (for 5.0 μm), ^{o}K	Mean-Molecular Velocity, $\times 10^{-4}$ m/sec	Time, sec
1	0.4313	343.44	2,199.48	2,166.32	0.12170	0.02667
2	0.2245	333.16	1,949.81	1,927.57	0.11380	0.13530
3	0.3681	468.47	1,583.63	1,572.61	0.10190	0.09841
4	0.3999	312.46	1,302.74	1,297.09	0.09209	0.03968
5	0.5287	307.37	1,234.89	1,215.32	0.08907	0.02968
6	0.5474	303.83	1,153.56	1,149.74	0.08659	0.02758
7	0.5656	303.79	1,092.72	1,089.53	0.08426	0.05512
8	0.5831	303.76	1,042.92	1,040.17	0.08231	0.02668

Table 6. Collection Efficiency

Fine Particle Radius, $x10^6$ m	η, Collection Efficiency (for 1.5 μm)	η, Collection Efficiency (for 5.0 μm)	ψ_{TOT}, Collection Efficiency
0.01	0.8324	0.2394	0.08384
0.02	0.8305	0.2388	0.08375
0.05	0.8252	0.2373	0.08356
0.10	0.8174	0.2350	0.08336
0.20	0.8049	0.2315	0.08301
0.50	0.7813	0.2247	0.08183

Table 7. Thermophoresis Velocity

Knudsen No., $x10^{-2}$	Thermophoresis Velocity (for 1.5 μm), m/sec	Thermophoresis Velocity (for 5.0 μm), m/sec
0.63870	0.9958	0.9370
0.31940	0.9939	0.9353
0.12770	0.9886	0.9303
0.06387	0.9806	0.9228
0.03194	0.9674	0.9103
0.01277	0.9415	0.8860

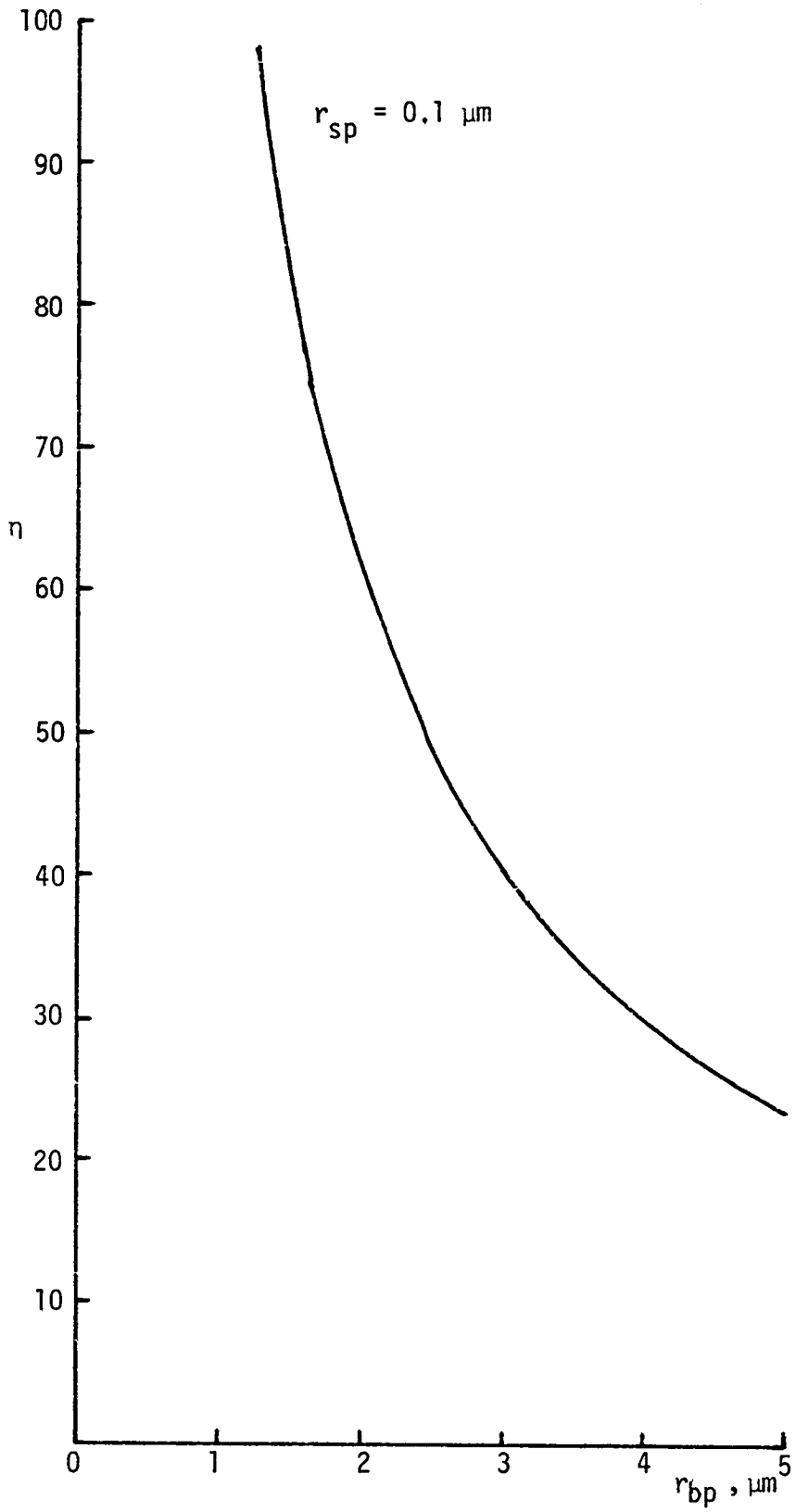

Figure 5. Collection efficiency versus large particle radius.

particle of 5 μm radius, η varies from 24 percent for fine particle radius 0.01 μm to 22 percent for fine particle radius 0.50 μm. Similarly, for a large particle radius of 1.5 μm, η varies from 83 percent for the fine particle radius 0.01 μm to 78 percent for the fine particle radius 0.5 μm. The trend shows in effect that the collection efficiency η is almost independent of the size of the fine particles, but depends on the size of the large particles. The values also indicate that there is a significant amount of agglomeration that is occurring.

The increase in the radius of the large particle due to agglomeration is not significant and hence, any effect on collection efficiency η due to radius increment is neglected.

However, collection efficiency, ψ_{TOT}, at the wall is small--it varies from 8.4 percent for fine particle radius 0.01 μm to 8.2 percent for fine particle radius 0.5 μm. The values are almost constant, indicating that ψ_{TOT} is independent of the size of the fine particles.

Figure 6 gives a comparative plot of the present model, Im's model, and particle size distribution obtained experimentally at The University of Tennessee Space Institute.

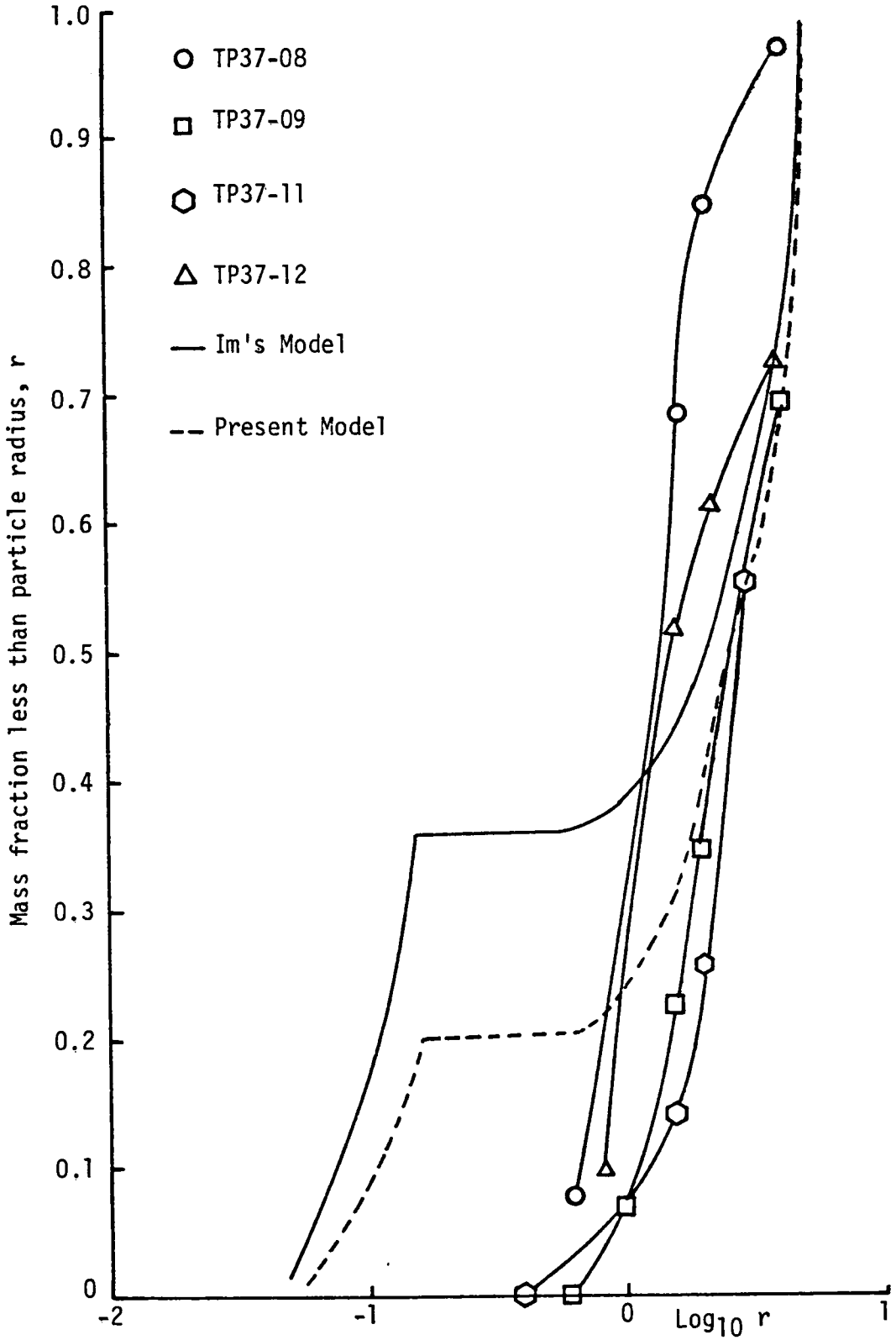

Figure 6. Particle size distribution of Im's model, the present model, and those obtained experimentally at UTSI.

CHAPTER V

CONCLUSIONS AND RECOMMENDATIONS

Conclusions

On comparing the plots, it can be concluded that a significant fraction of the fine particles has been removed. The model used is relatively simple and the process employed decreases the discrepancy that occurs between Im's theoretical prediction of particle size distribution and that obtained experimentally at The University of Tennessee Space Institute (UTSI).

Order of magnitude calculations have been described which show that other conceivable processes, such as agglomeration due to impaction in the turbulent flow or due to Brownian motion, have small consequences compared with the thermophoresis effect of small particles being attached to larger ones, at the temperature and flow conditions of interest here. The thermophoresis migration to the cool tube walls is not negligible, but this effect does not explain the relative growth of large particles, since submicron particles and those near one micron in size are collected almost equally at the wall.

Recommendations

There are several levels on which the work described here could be refined and extended.

1. A model might be developed which considers the thermophoresis effect, the turbulent impaction, and Brownian diffusion as acting simultaneously as mechanisms for collection of small particles on larger particles. At least the turbulent impaction could become more important at lower temperatures than considered here, for turbulent flow.
2. A more detailed gas-to-wall heat transfer calculation could be attempted, so as to obtain reliable axial temperature variations. The model could be modified to consider continuous temperature changes, rather than representing each component at an average temperature for thermophoresis calculations.
3. Calculations could be extended to components of the MHD apparatus downstream of the sampling section, if experimental measurements were available.
4. Although the measurements may be impractical, a measured particle size distribution at the diffuser inlet would be desirable, rather than using Im's calculations. Such measurements, if they verified Im's calculations, would also support the model described here.
5. Another conceivable coagulation effect which has not been discussed here is the effect of charging of the particles. In the combustor and generator, significant degrees of ionization exist. If some of the ions or electrons were captured by the particles, a charge imbalance is possible.

If some particles were oppositely charged, they would tend to be attracted to one another. The investigator, however, is not aware of any experimental or theoretical basis for attempting to predict the degree and sign of particle charging.

BIBLIOGRAPHY

BIBLIOGRAPHY

1. Im, K. H., and P. M. Chung. "Nucleation and Evolution of Slag Droplets in Coal Combustion," Proceedings of the Seventeenth Symposium on Engineering Aspects of Magnetohydrodynamics, Stanford, California, 1978. University, Mississippi: Dr. John Fox, Department of Mechanical Engineering, University of Mississippi, 1978. Pp. C.5.1-C.5.7.

2. Im, K. H., R. K. Ahluwalia, and G. F. Berry. "Analysis of Flow, Gas-Particle Radiation, and Particulate Deposition in Radiant Boilers," Argonne National Laboratory Report ANL/MHD-81-5, Argonne, France, April 1981.

3. Dicks, J. B., et al. "UTSI Quarterly Technical Progress Report: MHD Coal-Fired Flow Facility," Department of Energy Contract No. EX-76-C-01-1760, The University of Tennessee Space Institute, Tullahoma, Tennessee, July-September 1978.

4. Alstatt, M., et al. "UTSI Design Report for LMF Coal-Fired Facility (8 lb/sec): Nozzle, Supersonic Generator and Diffuser," Department of Energy Contract No. EX-76-C-01-1760, The University of Tennessee Space Institute, Tullahoma, Tennessee, June 1979.

5. Wang, H. H. "UTSI Topical Report: A Study of Seed Recovery and Particulate Emissions Control of the Coal-Fired Open-Cycle Magnetohydrodynamics/Steam Power Plant (CFFF)," Department of Energy Contract No. DE-AC02-79ET10815, The University of Tennessee Space Institute, Tullahoma, Tennessee, October 1980.

6. Fuchs, N. A. The Mechanics of Aerosols. New York: Pergamon Press, 1964.

7. Talbot, L., et al. "Thermophoresis of Particles in a Heated Boundary Layer," Journal of Fluid Mechanics, 101(Part 4):737-758, 1980.

8. Byers, R. Lee, and S. Calvert. "Particle Deposition from Turbulent Streams by Means of Thermal Force," Industrial and Engineering Chemistry Fundamentals, 8(No. 4):646-655, November 1969.

9. Brock, J. R. "On the Theory of Thermal Forces Acting on Aerosol Particles," Journal Colloid Science, 17:768-780, 1962.

10. Bird, R. B., W. E. Stewart, and E. N. Lightfoot. Transport Phenomena. New York: John Wiley and Sons, Inc., 1960.

11. Kreith, F. Principles of Heat Transfer. Second edition. Scranton, Pennsylvania: International Press, Inc., 1966.

12. Roy, G. D., and L. W. Crawford. "On Heat Balance in Coal-Fired MHD Systems, Channel Heat Transfer and Electrode Temperature Distributions." Paper No. 80-WA/HT-11, presented at American Society of Mechanical Engineers Meeting, Chicago, Illinois, November 16-21, 1980.

13. Im, K. H., and P. M. Chung. "Particulate Deposition from Turbulent Parallel Streams," Argonne National Laboratory Report ANL/MHD-81-2, Argonne, France, February 1981.

14. Schlichting, H. Boundary-Layer Theory. Sixth edition. New York: McGraw-Hill Book Company, 1968.

15. Kay, W. M., and M. E. Crawford. Convective Heat and Mass Transfer. Second edition. New York: McGraw-Hill Book Company, 1980.

16. Lanier, J., et al. "Topical Report: Secondary Combustor Evaluation Cell III Tests at UTSI," Department of Energy Contract No. EX-76-C-01-1760, The University of Tennessee Space Institute, Tullahoma, Tennessee, July 1979.

17. Gordon, S., and B. J. McBride. "Computer Program for Calculation of Complex Chemical Equilibrium Compositions, Rocket Performance, Incident and Reflected Shocks, and Chapman-Jouguet Detonations," National Aeronautics and Space Administration SP-273, Washington, D.C., 1971.

18. Hidy, G. M., and J. R. Brock. The Dynamics of Aerocolloidal Systems. First edition. New York: Pergamon Press, 1970.

19. Laufer, J. "The Structure of Turbulence in Fully Developed Pipe Flow," National Advisory Committee for Aeronautics Technical Report No. 1174, Washington, D.C., 1954.

APPENDICES

APPENDIX A

THE UNIVERSITY OF TENNESSEE SPACE INSTITUTE EXPERIMENTAL DATA AND IM'S MODEL

The University of Tennessee Space Institute Experimental Data

Table A.1 gives values for different mass flow rates for test runs TP37-08 to TP37-12.

Table A.1. UTSI Experimental Data

Test Run No.	$\dot{m}_{coal}$	$\dot{m}_{O_2}$	$\dot{m}_{N_2}$	$\frac{\text{Seed}}{\text{Coal}}$	Total Flow, lb-sec^{-1}	$\frac{\text{Coal}}{\text{Oxygen}}$
37-08	0.580	0.800	0.40	0.2049	1.78	0.602
37-09	0.610	0.750	0.40	0.2475	1.76	0.652
37-10	0.550	0.760	0.39	0.1779	1.70	0.614
37-11	0.500	0.825	0.40	0.1437	1.73	0.530
37-12	0.536	0.810	0.43	0.1111	1.78	0.596

Im's Model

Im et al. [1,2] have developed a technique that employs a complex physical model and numerical calculation of growth of droplets of slag and/or seed (potassium sulfate) due to nucleation and due to diffusion to existing particles. Typically, a significant fraction of the total particle mass comes to a radius in the neighborhood of 0.05 to 0.10 μm as a result of these calculations because of re-evaporation and condensation of particles which initially nucleate as 4-6x10^{-3} μm

particles. Im notes that the distribution is bimodal, with maximum number densities near 0.1 μm and near or above 1 μm radius. Thermophoresis as a mechanism of agglomeration of fine particles, which is considered in the preceding chapters of this study, is not included in the calculation by Im et al.

APPENDIX B

AGGLOMERATION OF FINE PARTICLES DUE TO TURBULENCE

Hidy and Brock [18] have developed an equation to describe the effect of turbulence and gravity on coagulation. The expression is for collisions per unit time per unit volume (collision rate density).

$$L_{ij}^{(T)} = 2\sqrt{2\pi}\, r_{ij}^2\, n_i\, n_j \left[\left(1 - \frac{\rho_g}{\rho_i}\right)^2 \left(A_j^{-1} - A_i^{-1}\right)^2 \overline{\left(\frac{Dq}{Dt}\right)^2} \right.$$

$$\left. + \frac{1}{9}\, r_{ij}^2\, \frac{\varepsilon_t}{\nu} + \frac{1}{3} \left(1 - \frac{\rho_g}{\rho_i}\right)^2 \left(A_j^{-1} - A_i^{-1}\right)^2 g^2 \right]^{1/2} . \qquad (B.1)$$

The first term in brackets arises due to differences in response of different sized particles to turbulent fluctuations; the second is due to random motions introduced by the variation in shear; and the third is due to different settling rates.

For large Reynolds number, Hidy and Brock [18] give

$$\overline{\left(\frac{Dq}{Dt}\right)^2} = 1.3\, \frac{\varepsilon_t^{3/2}}{\nu^{1/2}} , \qquad (B.2)$$

$$A_k = (B_k m_k)^{-1} = \frac{9}{2}\, \frac{\mu_g}{r_i^2\, \rho_i\, Cu} , \qquad (B.3)$$

where

B_k = mobility ,

m_k = mass of particle ,

Cu = Cunningham factor

$$= 1 + \frac{\lambda}{r_i}\left(A' + B'\, e^{-C'\frac{r_i}{\lambda}}\right).$$

For a length L of pipe,

$$\varepsilon_t = \frac{\bar{V}\,\frac{\pi D^2}{4}\,\Delta p}{\rho_g\,\frac{\pi D^2}{4}\,L}\ ; \qquad (B.4)$$

pressure drop,

$$\Delta p = \frac{\pi D\ \tau_w\ L}{\pi\,\frac{D^2}{4}}\ ; \qquad (B.5)$$

shear stress,

$$\tau_w = \frac{f}{2}\,\rho_g\,\bar{V}^2\ . \qquad (B.6)$$

Then,

$$\varepsilon_t = 4 \cdot \frac{f}{2} \cdot \frac{\bar{V}^3}{D}\ . \qquad (B.7)$$

For a typical case of $\dot{m}$ = 0.771 kg/sec,

$$D = 0.492 \text{ m} ,$$

$$T = 1{,}300^{\circ}\text{K} ,$$

$$\rho_g = 3\times10^{-4} \text{ gm cm}^{-3} ,$$

$$\rho_i = 2.5 \text{ gm cm}^{-3} ,$$

$$\mu_g = 5\times10^{-4} \text{ gm cm}^{-1} \text{ sec}^{-1} ,$$

$$\bar{V} = 1{,}330 \text{ cm sec}^{-1} ,$$

$$\nu = 1{,}6 \text{ cm}^2/\text{sec} ,$$

$$Re = 40{,}000 .$$

From Eq. (B.7),

$$\varepsilon_t = 5.28\times10^{5} \text{ cm}^2 \text{ sec}^{-3} ,$$

$$\frac{\rho_g}{\rho_i} \approx 0 .$$

For $r_i = 0{,}1$ μm,

$$\frac{1}{A_i} = 7.2\times10^{-7} \text{ sec} ;$$

for $r_j = 2.0$ μm,

$$\frac{1}{A_j} = 5.4\times10^{-5} \text{ sec} .$$

In Eq. (B.1),

$$\text{first term in bracket} = 1.0966 \text{ cm}^2 \text{ sec}^{-2} ,$$

$$\text{second term in bracket} = 1.552\times10^{-3} \text{ cm}^2 \text{ sec}^{-2} ,$$

$$\text{third term in bracket} = 9.09\times10^{-4} \text{ cm}^2 \text{ sec}^{-2} .$$

Thus, only the first term is important. Hence,

$$L_{ij}^{(T)} = (1.097)^{1/2}\, 2\sqrt{2\pi}\, (2.1\times10^{-4})\, n_i\, n_j$$

$$L_{ij}^{(T)} = 2.316\times10^{-7}\ \frac{cm^3}{sec}\ n_i\, n_j\ . \qquad (B.8)$$

If $\omega_j = 0.04$,

$$n_j = \frac{0.04\ \rho_g}{m_j}$$

$$= 1.43\times10^{5}\ \text{particle/cm}^3\ .$$

Then, using Eq. (B.8),

$$-\frac{1}{n_i}\frac{dn_i}{dt} = 2.316\times10^{-7} \cdot 1.43\times10^{5}$$

$$-\frac{1}{n_i}\frac{dn_i}{dt} = 0.0338\ . \qquad (B.9)$$

Integrating Eq. (B.9),

$$\frac{n_i}{n_{io}} = e^{-0.0338\,t}\ , \qquad (B.10)$$

and for flow time 0.4 sec,

$$\frac{n_i}{n_{io}} = 0.9866\ .$$

Thus, the fraction of particles collected due to turbulence equals 1 - 0.9866 = 0.0134. This value is obtained for large particle radius 2 μm.

For large particle radius 4 μm, n_i/n_{io} = 0.9770 after 0.4 sec. Thus, somewhere in the range of 2 percent of the small particles will be collected by large particles due to turbulence effects.

APPENDIX C

NUSSELT NUMBER IN TURBULENT GAS SYSTEM

It is required to show that Eq. (3,4) reduces to Eq. (3.5) for the particle size range and turbulence conditions relevant to the present study.

Consider response of a particle to a sinusoidal velocity field. Let

u_p = velocity of the particle ,

u_o = maximum gas velocity ,

ϕ = lag ,

f' = frequency of oscillation ,

Cu = Cunningham factor ,

velocity $u = u_o \sin \omega t$,

force balance,

$$m_p \frac{du_p}{dt} = - \frac{6\pi\mu_g r}{Cu} (u_p - u) , \qquad (C.1)$$

$$\frac{du_p}{dt} + \frac{6\pi\mu_g r}{m_p Cu} u_p = \frac{6\pi\mu_g r}{m_p Cu} u . \qquad (C.2)$$

According to Hidy and Brock [18],

$$A = \frac{6\pi\mu_g r}{m_p Cu}$$

is the reciprocal relaxation time. Then,

$$\frac{du_p}{dt} + Au_p = Au_o \sin \omega t \ . \tag{C.3}$$

On integrating Eq. (C.3) and applying at $t = 0$, $u_p = 0$,

$$\frac{u_p}{Au_o} = \frac{A}{A^2 + \omega^2} \sin \omega t - \frac{\omega}{A^2 + \omega^2} \cos \omega t + \frac{\omega\, e^{-At}}{A^2 + \omega^2} \ . \tag{C.4}$$

The last term in Eq. (C.4) dies out as $t \to \infty$.

Let

$$\frac{A}{\sqrt{A^2 + \omega^2}} = \cos \phi \ ,$$

then,

$$\sin \phi = \frac{\omega}{\sqrt{A^2 + \omega^2}} \ .$$

Then Eq. (C.4) reduces to

$$\frac{u_p}{u_o} = \frac{A}{\sqrt{A^2 + \omega^2}} \sin(\omega t - \phi) \ , \tag{C.5}$$

where ϕ is defined as

$$\phi = \cos^{-1} \frac{A}{\sqrt{A^2 + \omega^2}} ,$$

and relative velocity,

$$\left|\frac{u_p}{u_o}\right| = \frac{A}{\sqrt{A^2 + \omega^2}} .$$

Equation (C.5) can be modified to

$$\frac{u_p}{u_o} - \sin \omega t = \frac{A}{\sqrt{A^2 + \omega^2}} \sin(\omega t - \phi) - \sin \omega t . \qquad (C.6)$$

In the following, the rms velocity difference between a particle and gas will be evaluated for substitution into a Reynolds number.

$$\frac{u_p - u_o \sin \omega t}{u_o} = \frac{1}{\sqrt{1 + \omega^2 A^{-2}}} \sin(\omega t - \phi) - \sin \omega t . \qquad (C.7)$$

$$A = \frac{6\pi\mu_g r}{m_p Cu}$$

can be simplified to

$$A = \frac{9}{2} \frac{\mu_g}{r^2 \rho_p Cu} .$$

Squaring Eq. (C.7),

$$\left(\frac{u_p - u_o \sin \omega t}{u_o}\right)^2 = \frac{1}{1+\omega^2 A^{-2}} \sin^2(\omega t - \phi) - \frac{2 \sin(\omega t - \phi)\sin \omega t}{\sqrt{1+\omega^2 A^{-2}}} + \sin^2 \omega t \, . \qquad (C.8)$$

Integrating Eq. (C.8) from t = 0 to t = $2\pi/\omega$,

$$\int_0^{2\pi/\omega} \left(\frac{u_p - u_o \sin \omega t}{u_o}\right)^2 dt = \frac{1}{1+\omega^2 A^{-2}} \int_0^{2\pi/\omega} \left[1 - \cos 2(\omega t - \phi)\ dt\right] - \frac{2}{\sqrt{1+\omega^2 A^{-2}}} \int_0^{2\pi/\omega} \sin(\omega t - \phi)\sin \omega t \, dt + \frac{1}{2} \int_0^{2\pi/\omega} \frac{1}{2} (1 - \cos 2 \omega t)\, dt \, . \qquad (C.9)$$

This simplifies to

$$\frac{\int_0^{2\pi/\omega} \left(\frac{u_p - u_o \sin \omega t}{u_o}\right)^2 dt}{\int_0^{2\pi/\omega} dt} = \frac{1}{2}\left(1 - \frac{1}{1+\omega^2 A^{-2}}\right) . \qquad (C.10)$$

Mean square velocity difference is

$$\overline{(u_p - u_g)^2} = \frac{u_o^2}{2}\left(1 - \frac{1}{1+\omega^2 A^{-2}}\right) . \qquad (C.11)$$

Define a Reynolds number,

$$Re_v = \frac{D_{bp}\sqrt{(u_p - u_g)^2}}{\nu} . \qquad (C.12)$$

According to energy spectra figures given by Laufer [19],

$$\overline{u'}^2 = \int_0^\infty F_a(K_1)\, dK_1 , \qquad (C.13)$$

where

K_1 = wave number = $1/\lambda'$,

λ' = wavelength .

Most energy lies between $K_1 = 0.1$ and $K_1 = 1$ cm^{-1}. Consider $K_1 = 1$ cm^{-1}; hence, $f' = 1\ u'$. As measured by Laufer, $u' \approx V^*$ in the turbulent core.

For Re = 50,000,

$$V^* \approx 0.05\ \overline{V} ,$$

$$\overline{V} \approx 1{,}300 \text{ cm/sec} ,$$

$$V^* \approx 65 \text{ cm/sec} .$$

Then,

$$f' = \frac{\omega}{2\pi} = 65(1) \text{ sec}^{-1} ,$$

$$\omega = 2\pi\ (65) \text{ sec}^{-1} .$$

For $r = 1\ \mu m$, $\lambda = 0.35\ \mu m$,

$$Kn = 0.35 ,$$

$$Cu = 1.43 ,$$

$$A^{-1} = 0.17 \times 10^{-4} \text{ sec} ,$$

$$\omega A^{-1} = 0.0069 .$$

Thus,

$$\overline{(u_p - u_g)^2} = \frac{u_o^2}{2}\left(1 - \frac{1}{1 + (0.0069)^2}\right) ,$$

$$u_o = \sqrt{2V^*} ,$$

$$\left(\overline{(u_p - u_g)^2}\right)^{1/2} \approx (0.0069)(65) .$$

Thus, Eq. (C.12) reduces to

$$Re_v \approx 10^{-4} .$$

Thus, Eq. (3.4) reduces to

$$Nu = 2.0 ,$$

which is Eq. (3.5) used for the purpose of calculation.

For $\lambda = 5\ \mu m$, $\lambda = 0.35\ \mu m$,

$$Kn = 0.07 ,$$

$$Cu = 1.084 ,$$

$$A^{-1} = 3.22 \times 10^{-4} \text{ sec} ,$$

$$(\omega A^{-1}) = 0.1315 .$$

Thus,

$$\left(\overline{(u_p - u_g)^2}\right)^{1/2} \approx (0.1303)(65) \ .$$

Thus, Eq. (C.12) reduces to

$$Re_v \approx 5x10^{-3} \ ,$$

and hence, Eq. (3.4) reduces to

$$Nu = 2.02 \ ,$$

which is only 1 percent greater than the stagnant value of Nu = 2.

For the purposes of calculation in this study, use of Nu = 2 appears to be sufficiently accurate to estimate the temperature difference of the large particles and surrounding gas.

APPENDIX D

TEMPERATURE PROFILE IN MAGNETOHYDRODYNAMIC COMPONENTS

The assumption of a linear temperature profile in various components for calculation of flow time is justified on the grounds that the error involved in doing so is not more than 1 percent when compared to a more sophisticated calculation.

In Eq. (3.17), there is the expression

$$\int_{x_1}^{x_2} \frac{dx}{T} .$$

If it is assumed that

$$T = a + bx , \tag{3.18}$$

$$T = T_1 + (T_2 - T_1)\frac{x}{L} . \tag{D.1}$$

Differentiating Eq. (D.1),

$$dx = \frac{L\, dT}{T_2 - T_1} . \tag{D.2}$$

If, on the other hand,

$$\dot{q}'' = h(T - T_w) , \tag{D.3}$$

with h (heat transfer coefficient) constant, then

$$\dot{m}\, C_p \frac{dT}{dx} = - P'h\,(T - T_w)\ , \qquad (D.4)$$

where

$$P' = \text{perimeter}\ .$$

From Eq. (D.4),

$$dx = - \frac{\dot{m}\, C_p}{P'h} \frac{dT}{T - T_w}\ . \qquad (D.5)$$

On integrating Eq. (D.5),

$$x = - \frac{\dot{m}\, C_p}{P'h} \ell n\,(T - T_w) + C\ , \qquad (D.6)$$

where C = constant of integration.

At $x = 0$, $T = T_1$, then

$$\frac{T - T_w}{T_1 - T_w} = e^{- \frac{P'h}{\dot{m}\, C_p} x}\ . \qquad (D.7)$$

Also,

$$\frac{T_2 - T_w}{T_1 - T_w} = e^{- \frac{P'h}{\dot{m}\, C_p} L}\ , \qquad (D.8)$$

where L = length of the component.

Therefore,

$$\frac{T - T_w}{T_1 - T_w} = \left(\frac{T_2 - T_w}{T_1 - T_w} \right)^{x/L}\ . \qquad (D.9)$$

On differentiation,

$$dx = \frac{L}{T - T_w} \left[\ell n \frac{T_2 - T_w}{T_1 - T_w} \right]^{-1} dT \ . \qquad (D.10)$$

Integration Eq. (D.10),

$$\int_{x_1}^{x_2} \frac{dx}{T} = \int_{T_1}^{T_2} \frac{L}{\ell n \frac{T_2 - T_w}{T_1 - T_w}} \frac{dT}{T(T - T_w)} \ , \qquad (D.11)$$

$$\int_{x_1}^{x_2} \frac{dx}{T} = \frac{L}{\ell n \frac{T_2 - T_w}{T_1 - T_w}} \left(\frac{1}{T_w} \right) \left[\ell n \left(\frac{T_2 - T_w}{T_1 - T_w} \right) - \ell n \frac{T_2}{T_1} \right] . \qquad (D.12)$$

One needs to compare

$$\overline{\left(\frac{1}{T} \right)}_1 = \frac{1}{L} \int \frac{dx}{T} = \frac{\ell n \ T_2/T_1}{T_2 - T_1} \qquad (D.13)$$

for the linear assumption. And

$$\overline{\left(\frac{1}{T} \right)}_2 = \frac{1}{L} \int \frac{dx}{T} = \frac{1}{T_w} \left[1 - \frac{\ell n \ T_2/T_1}{\ell n \frac{T_2 - T_w}{T_1 - T_w}} \right] \qquad (D.14)$$

for the case with constant heat transfer coefficient.

To compare the limits of Eqs. (D.13) and (D.14) for small values of $(T_2 - T_1)$, $\ell n \ y$ can be expressed as

$$\ell n\ y = 2\left(x + \frac{x^3}{3} + \frac{x^5}{5} + \ldots\right) , \tag{D.15}$$

where

$$x = \frac{y - 1}{y + 1} ;$$

$$\ell n\ \frac{T_2}{T_1} = 2\left[\frac{T_2 - T_1}{T_2 + T_1} + \frac{1}{3}\left(\frac{T_2 - T_1}{T_2 + T_1}\right)^3 + \ldots\right] , \tag{D.16}$$

$$\ell n\ \frac{T_2 - T_w}{T_1 - T_w} = 2\left[\frac{T_2 - T_1}{T_2 + T_1 - 2T_w} + \frac{1}{3}\left(\frac{T_2 - T_1}{T_2 + T_1 - 2T_w}\right)^3 + \ldots\right] . \tag{D.17}$$

If $T_2 - T_1 \ll T_2 + T_1$ and $(T_2 - T_1) \ll T_2 + T_1 - 2\,T_w$, then

$$\overline{\left(\frac{1}{T}\right)}_1 \approx \frac{2}{T_1 + T_2} \tag{D.18}$$

$$\overline{\left(\frac{1}{T}\right)}_2 \approx \frac{2}{T_1 + T_2} . \tag{D.19}$$

Thus, in the limit of small $T_2 - T_1$, and T_w not too close to T_1 and T_2, one can use mean temperature

$$\frac{1}{L}\int_{x_1}^{x_2} \frac{dx}{T} \approx \frac{1}{T_{av}} , \tag{D.20}$$

where

$$T_{av} = \frac{T_1 + T_2}{2} .$$

To evaluate the discrepancy for the largest value of $(T_2 - T_1)$, for component 3,

$$T_2 = 2{,}430^{o}R \ ,$$

$$T_1 = 3{,}285^{o}R \ ,$$

$$T_w = \ 844^{o}R \ ,$$

$$\frac{1}{T_{av}} = 3.50\text{x}10^{-4} \ {}^{o}R^{-1} \ , \tag{D.21}$$

$$\frac{\ell n \ T_2/T_1}{T_2 - T_1} = 3.526\text{x}10^{-4} \ {}^{o}R^{-1} \ , \tag{D.22}$$

$$\frac{1}{T_w}\left(1 - \frac{\ell n \ T_2/T_1}{\ell n \ \frac{T_2 - T_w}{T_1 - T_w}}\right) = 3.564\text{x}10^{-4} \ {}^{o}R^{-1} \ . \tag{D.23}$$

Percentage error between Eqs. (D.21) and (D.23)

$$= 1.8 \text{ percent} \ .$$

Percentage error between Eqs. (D.22) and (D.23)

$$= 1.0 \text{ percent} \ .$$

Because the linear temperature profile (in the axial direction) is used only to calculate flow time, it is contended that the linear assumption is superior to use of an average temperature, and gives results sufficiently close to those of a more sophisticated analysis to justify the use of the linear profile assumption.

APPENDIX E

INVERSE SQUARE RULE FOR THERMOPHORETIC VELOCITIES

Equations have been formulated to show that thermophoretic velocity at a distance R from the center of a large particle is proportional to the inverse square of R and, hence, leads to Eq. (3.24).

$$\text{Heat flux, } \dot{q}'' = - k_g \frac{dT}{dR} . \tag{E.1}$$

$$\text{Heat flow, } \dot{q} = 4\pi R^2 \dot{q}'' . \tag{E.2}$$

Equating Eqs. (E.2) and (E.1) and rearranging,

$$\frac{dR}{R^2} = - k_g \frac{4\pi dT}{\dot{q}} . \tag{E.3}$$

Integrating Eq. (E.3) and applying at $R = r_{bp}$, $T = T_p$,

$$\frac{1}{R} - \frac{1}{r_{bp}} = \frac{4\pi k_g}{\dot{q}} (T - T_p) . \tag{E.4}$$

As $R \to \infty$, $T = T_g$, then Eq. (E.4) reduces to

$$- \frac{1}{r_{bp}} = \frac{4\pi k_g}{\dot{q}} (T_g - T_p) , \tag{E.5}$$

$$\dot{q} = - 4\pi k_g (T_g - T_p) r_{bp} , \tag{E.6}$$

$$\frac{dT}{dR} = - \frac{\dot{q}}{4\pi R^2} \cdot \frac{1}{k_g} , \tag{E.7}$$

$$\frac{dT}{dR} = \frac{4\pi r_{bp} \, k_g \, (T_g - T_p)}{4\pi R^2 \, k_g} , \tag{E.8}$$

$$\left.\frac{dT}{dR}\right|_R = \frac{r_{bp} \, (T_g - T_p)}{R^2} , \tag{E.9}$$

$$\left.\frac{dT}{dR}\right|_{r_{bp}} = - \frac{T_p - T_g}{r_{bp}} , \tag{3.8}$$

$$\frac{\left.\frac{dT}{dR}\right|_R}{\left.\frac{dT}{dR}\right|_{r_{bp}}} = + \frac{r_{bp}^2}{R^2} , \tag{E.10}$$

$$U_T\Big|_R \; \alpha \; \frac{dT}{dR} . \tag{E.11}$$

Thus,

$$\frac{dR}{dt} = - U_T \frac{r_{bp}^2}{R^2} . \tag{3.24}$$

APPENDIX F

RATIO OF PARTICLE AND GAS MASS

Calculations are done in order to show that the approximation $m_p/m_g \approx 0.04$ is a valid one and not arbitrary.

From coal analysis, there is 15 percent ash in coal.

$$\text{Coal flow rate} = 0.5 \text{ lb/sec} ,$$

$$\dot{m} = 1.7 \text{ lb/sec} ,$$

$$\frac{m_p}{m_g} = \frac{0.5 \cdot 0.15}{1.7} \approx 0.04 .$$

APPENDIX G

FRACTION OF FINE PARTICLES COLLECTED BY LARGE PARTICLES DUE TO THERMOPHORESIS

Table G.1 gives the overall mass fraction of fine particles collected by large particles and also the total fraction of fine particles collected. Increase in radius of large particles having undergone agglomeration is also noted.

$$\sum \frac{\omega_{A'}}{0.64} (0.36)\ \eta_i = 0.152909 \ .$$

Mass fraction of small particles collected

$$= \frac{0.152909}{0.36}$$

$$= 0.4247 \ ,$$

which is 42.47 percent.

Table G.1. Data Obtained by the Present Model

r, μm	η_i	ω_A'	$\omega_A'/0.64\ (0.36)\ \eta_i$	$\delta r_i/r_i$
0.70 to 1.25	0.9887	0.0375	0.020860	0.1588
1.25 to 1.75	0.8213	0.0500	0.023099	0.1350
1.75 to 2.25	0.6121	0.0700	0.024101	0.1037
2.25 to 2.75	0.4867	0.0575	0.015742	0.0840
2.75 to 3.25	0.4031	0.0475	0.010770	0.0705
3.25 to 3.75	0.3434	0.055	0.010624	0.0606
3.75 to 4.25	0.2987	0.135	0.022683	0.0531
4.25 to 4.75	0.2640	0.095	0.014108	0.0472
4.75 to 5.00	0.2427	0.080	0.010922	0.0436

APPENDIX H

AN EXPRESSION FOR PARTICLE CONCENTRATION RATIO

When evaluating collection efficiency, ψ, it has been noted

$$\frac{C_A}{C_{A_0}} = \exp\left[- \frac{J}{C_A} \cdot \frac{4}{D} \cdot \frac{x}{\overline{V}} \right] . \tag{3.64}$$

Equations are formulated and evaluated to obtain Eq. (3.64). Assume J/C_A to be constant in a given component

$$\text{inflow} = C_A \overline{V} A , \tag{H.1}$$

$$\text{outflow} = C_A \overline{V} A + \frac{d}{dx}(C_A \overline{V} A) dx , \tag{H.2}$$

$$\text{deposition} = J P' dx , \tag{H.3}$$

where perimeter, $P' = \pi D$,

$$\text{inflow} = \text{outflow} + \text{deposition} . \tag{H.4}$$

On substitution and rearrangement,

$$- \frac{d C_A}{dx} = \frac{J P'}{\overline{V} A} , \tag{H.5}$$

$$- \frac{d C_A}{dx} = \frac{J}{\overline{V}} \cdot \frac{4}{\pi D^2} \cdot \pi D , \tag{H.6}$$

$$- \frac{d C_A}{dx} = \frac{J}{\overline{V}} \cdot \frac{4}{D} , \tag{H.7}$$

$$-\frac{dC_A}{C_A} = \frac{J}{C_A} \cdot \frac{4}{D} \cdot \frac{dx}{\bar{V}} \quad . \tag{H.8}$$

Integrating Eq. (H.8) from $C_A = C_{A_0}$ to C_A and $x = 0$ to x,

$$\frac{C_A}{C_{A_0}} = \exp\left[-\frac{J}{C_A} \cdot \frac{4}{D} \cdot \frac{x}{\bar{V}}\right] \quad . \tag{3.64}$$

VITA

Jawaharlal Prasad was born in Pirganj (District of Samastipur, Bihar), India, on May 2, 1957. He attended St. Xavier's School, Sahibganj, and passed the Indian School Certificate Examination securing a first division. He joined the Indian Institute of Technology, Kanpur, in July 1974 to pursue studies towards the degree of Bachelor of Technology with a major in Chemical Engineering and received this degree in April 1979.

In June 1980, Mr. Prasad entered The University of Tennessee Space Institute and completed the requirements for the Master of Science degree in Chemical Engineering in August 1981. Beginning in September 1981, he plans to study towards a Ph.D. degree in Chemical Engineering at The University of Tennessee, Knoxville.